BAO measurement and cosmological parameter constraints using eBOSS galaxies and voids

Daniel Felipe Forero Sánchez
daniel.forerosanchez@epfl.ch

Supervisor: Cheng Zhao

Professor: Jean-Paul Kneib

December 25, 2019

Abstract

Baryon Acoustic Oscillations (BAO) are a signal imprinted in the 3-dimensional distribution of various tracers in the Universe. It provides a standard scale that can be measured at different redshifts. In the present work, we aim to use the eBOSS survey ELG tracers and the large ($R > 16\,h^{-1}$Mpc) cosmic voids to measure the BAO scale in the redshift range of $0.6 < z < 1.1$. Nonetheless, the observed BAO signal obtained from the voids is not significant enough for it to improve the measurement that can be obtained from the galaxy BAO. Additionally, the two-point correlation functions show unaccounted for systematical effects in the survey. These are more prominent in the galaxy and small void ($R < 8\,h^{-1}$Mpc) distributions, than they are in the large voids'.

Contents

1 Introduction **3**

2 Background theory **3**

2.1 Baryon Acoustic Oscillations . . . 3

2.2 Voids . . . 4

2.3 Systematical Effects . . . 5

2.3.1 Fiber collisions . . . 5

2.3.2 Redshift Failures . . . 5

2.3.3 Angular photometric systematics . . . 6

2.3.4 Normalization and FKP weights . . . 6

2.3.5 Applying systematic weights . . . 6

2.4 DIVE . . . 7

2.5 Types of voids . . . 7

2.6 The eBOSS survey . . . 8

3 Method **8**

3.1 Pipeline . . . 9

3.2 SNR analysis for BAO feature . . . 10

3.3 Fitting procedure . . . 11

3.3.1 The model . . . 11

3.3.2 Parameter inference . . . 12

4 Results **12**

4.1 ELG . . . 12

5 Conclusion **12**

References **13**

1 Introduction

Baryon Acoustic Oscillations (BAO) provide a *standard ruler* or scale that can be tracked at different redshifts, its measurement is then of This is due to the fact that it allows us to further improve the constraints on cosmological parameters (Bassett et al., 2010). The signal is encoded in the spatial distribution of matter in the Universe. Traditionally, different kinds of massive cosmic objects or *tracers*, as well as the anisotropies in the Cosmic Microwave Background (CMB) are used to measure the scale. This work aims towards the measurement of the BAO peak by combining Emission Line Galaxies (ELG) and the voids in their distribution (see section 2.2), following previous work by Zhao et al. (2018).
In section 2 we discuss the basics of the BAO phenomenon and the use of cosmic voids as tracers of under-densities. Section 3 discusses the method used to analyze the data, including the software to generate the void catalogs from a given galaxy one. Then, section in section **??** we show the obtained results for different tracers, while in section **??** we discuss them. Finally, we state the conclusions of the study and mention some future directions.

2 Background theory

2.1 Baryon Acoustic Oscillations

Nowadays, the baryonic matter of the Universe can be roughly distributed in a 75% hydrogen and a 25% helium. Nevertheless, before we had these elements, in the early Universe, the temperature was high enough for the protons and electrons to be found separately: at this stage we had an ionized plasma. The components of this plasma were electrically charged, thus, electromagnetically interacting with the photon gas, whose short mean free path made the Universe optically thick. In addition to the ionized plasma, dark matter was also present at these early stage.
The behavior of small matter density anomalies δ is described by equation 1. Notice that it has the form of an oscillator. These are what we call *Baryon acoustic oscillations* (BAO). These are entirely dependent on the coupling between baryonic matter and photons.

$$\ddot{\delta} + 2H\dot{\delta} + \left\{\frac{c_s^2 k^2}{a^2} - 4\pi G\rho\right\}\delta = 0 \tag{1}$$

Notice the factor in braces has a *pressure term* $\left(\frac{c_s^2 k^2}{a^2}\right)$ and a *gravitational term*, $(4\pi G\rho)$. The oscillatory behavior is expected as long as $\frac{c_s^2 k^2}{a^2} > 4\pi G\rho$. This inequality also holds without gravity, however, its presence implies that the oscillations will be dampened and that if $k = a\frac{\sqrt{4\pi G\rho}}{c_s} \equiv k_J$ (Jeans' wavenumber), the oscillation frequency would be zero. This tells us that at small scales ($k > k_J$), pressure dominates and drives the oscillatory behavior, while at large scales ($k < k_J$), the gravitational term will dominate and fluctuations will simply grow (Baumann, n.d.).
Additionally, it is imperative that the baryonic plasma is coupled (electromagnetically) to the photon gas for this process to be carried on. Therefore, this phenomenon will stop happening when such coupling disappears. This happens at the age of recombination, when the hydrogen

is formed (and not destroyed by high-energy photons) and the baryonic gas becomes neutral, hence, transparent to the photons. This, in turn, implies that these oscillations were "frozen" at time $t_{rec} \approx 4 \times 10^5\,\mathrm{yr}$, while the previously decoupled photon gas was free to leave, forming the CMB. This, rather well-known time, combined with the speed at which this pressure waves moved, can be used to define a *standard ruler* or a characteristic scale (Eisenstein et al., 1998; Eisenstein et al., 2007), that is, a standard angular distance that can be accurately measured at different redshifts.

It is possible to compute the distance at which these oscillations were frozen, a.k.a. the *sound horizon*, more formally defined as the comoving distance the sound waves travel from $t = 0$ to $t = t_{rec}$ (Weinberg et al., 2013). This quantity can be easily computed knowing that the comoving distance travelled with speed c_s is

$$\chi_s = \int_0^{t_{rec}} \frac{c_s(t)}{a(t)} \mathrm{d}t. \tag{2}$$

In our case, $c_s = c/\sqrt{3(1+R)}$ with $R \equiv 3\rho_b/\rho_\gamma$ (Eisenstein et al., 1998; Dodelson, 2003) and the result is $\chi_s \approx 150\,\mathrm{Mpc}$ (Weinberg et al., 2013). Once the photon gas decoupled, the remaining BAO peak continued to interact gravitationally with the dark matter, so we expect the latter to also show such characteristic, see figure 1 in Eisenstein et al. (2007).

Then, this BAO signature is imprinted both in the characteristic size of the temperature anomalies of the CMB and in the clustering of galaxies. The analysis of the former yields values of $\chi_s(z_{rec}) = (146.8 \pm 1.8)\,\mathrm{Mpc}$ and $\chi_s(z_{drag}) = (153.3 \pm 2.0)\,\mathrm{Mpc}$ (Komatsu et al., 2009). In the latter case, the sound horizon can be statistically extracted from the 3D distribution of galaxies by means of the *two-point correlation function* (2PCF), this is, the histogram of the separations between a pair of galaxies (Peebles, 1980; Eisenstein et al., 2005). A nice illustration can be found in figure 1.5 of Bassett et al. (2010), alongside a thorough explanation on how the signal is encoded in the tracer distribution.

As explained before, the BAO phenomenon, and the signal, is inherent to the matter distribution in the Universe. This means that a variety of different tracers can be used to extract the signal. This is rather convenient when looking for it at different redshifts. Some previously used tracers are quasars (McDonald et al., 2006; Ata et al., 2018), galaxies (Eisenstein et al., 2005) and galaxy clusters (T. Hong et al., 2012; Tao Hong et al., 2016). Recent studies (Kitaura et al., 2016; Liang et al., 2016; Zhao et al., 2018) evaluate the possibility to use cosmic voids as tracers, too.

2.2 Voids

Given that the BAO signal is encoded in the distribution of galaxies or *matter tracers*, we can expect to be able to get information from the distribution of the underdensities or *voids*. However, the definition of voids is rather difficult and depends strongly on the matter tracer used (van de Weygaert et al., 2009). The many possible definitions of this kind of structure has produced different kinds of void-finding algorithms. As stated by Zhao et al. (2016), we can outline some common definitions of voids as follows.

Colberg et al. (2005) define voids as regions with mean overdensity of at most -0.8. Such

regions are minima of the smoothed initial density field, where spheres are located and subsequently merged according to a set of rules (see reference for details) to form the final voids. A second approach is that of Hahn et al. (2007) and Forero-Romero et al. (2009), in which the definition of void is given by the local gravitational evolution as given by halo dynamics. Abel et al. (2012) analyze the cosmic web in phase space and classify regions according to the DM stream density. Voids are defined as particles that record being part of only their primordial stream (see figure 5, top-left panel in the reference). Finally, voids can be regarded as simply the empty regions in the spatial distribution of tracers. Among these, the first three depend on free parameters such as the smoothing scale of the density field (Hahn et al., 2007). Either way, all definitions agree on voids being underdensities. It is this what makes them less vulnerable to non-linearities in the gravitational evolution of the Universe (van de Weygaert et al., 2009; Zhao et al., 2016).

2.3 Systematical Effects

SEE WHICH IS THE PAPER THAT DESCRIBES THESE, INFO TAKEN FROM THE README MEANWHILE

2.3.1 Fiber collisions

For the targets' spectra to be observed, each should be assigned a fiber. When two targets are too close (less than $r_{cp} \equiv 62''$), they can't be observed by the same plate, at the same time. In this case, only one of them is selected for measurement, however, the others' spectra could be measured by another plate. (NOT SURE IF THIS DEFINITION IS NECESSARY) The *tiling success rate* (TSR), defined over each sector as the number of measured targets over the number of targets quantifies this effect. (PUT TSR PLOT AS EXAMPLES?)
Collision groups are defined as (ARNAUD) sets of targets within the fiber collision radius, r_{cp} that couldn't be observed by any plate. The *close-pair weight*, w_{cp} is defined (per collision group) as the total number of targets over the number of observed ones. By applying this weight to the resolved objects, unobserved targets are accounted for in the final catalog.

2.3.2 Redshift Failures

The success rate of the spectroscopy pipeline (SSR) is not 100%. It can be affected by factors such as observation conditions and position of the fiber in the focal plane. (Arnaud) defines the redshift failure weight, w_{noz} to take into account both these effects by estimating the SSR based on the median signal to noise ratio, $\mathrm{SSR_{obs}}$, and the position in the focal plane $\mathrm{SSR_{pos}}$. In this way,

$$w_{noz} \equiv (\mathrm{SSR_{obs}SSR_{pos}})^{-1}.$$

2.3.3 Angular photometric systematics

Various effects are grouped under this category. Each is represented in a HEALPIX map by the galactic extinction, H I column density, Gaia stellar density, DECaLS depth and seeing parameters, hereon p_i. A multilinear fit to the model

$$y^k = \epsilon + \sum_i c_i p_i^k$$

is performed for all p_i^k using a squared error loss. The fit is done per chunk in the survey, this is eboss21, eboss22, eboss23 and eboss25. The first two are the SGC, while the other are in the NGC. The index k then labels the pixels in the chunk.
The weights designed to partially correct for these effects are defined as

$$w_{\text{systot}} = \left(y^k\right)^{-1}.$$

2.3.4 Normalization and FKP weights

To effectively apply the weights, the mean of w_{systot} over all ELG objects in the chunk is normalized to one.
The completeness weights are then computed as

$$w_{\text{comp}} = w_{\text{systot}} w_{cp} w_{noz}.$$

The redshift failure weight is normalized too, such that the mean of w_{comp} over objects with reliable spectroscopic measurement and stars (with $w_{noz} = 1$) is the same as the mean of w_{comp} over valid ELGs.
Invalid objects such as those with no reliable redshift or with a collided fiber are zero-weighted by setting $w_{noz} = 0$ and w_{cp} respectively.
The final clustering sample is obtained after selecting objects with SSR ≥ 0, $z \in (0.6, 1.1)$ and completeness (number of resolved fibers over number of objects, per sector) greater than 50%.
Due to the dependence of the tracer number density $n(z)$ on the redshift, we must apply too a final weight

$$w_{\text{FKP}} \equiv \frac{1}{1 + n(z) P_0}; \quad P_0 = 4000\, h^{-3}\text{Mpc}^3.$$

2.3.5 Applying systematic weights

Through the application of the weighing schemes previously mentioned, we are able to control the systematic effects present in the final catalog. To partially apply systematics we proceed as follows:

- We compute $w_{\text{comp}}^{\text{ALLSYST}} = w_{\text{systot}} w_{cp} w_{noz} w_{\text{FKP}}$ and the effective number of tracers in each chunk

  $$n_{eff} = \sum_{i=1}^{N_{chunk}} w_{\text{comp},i}^{\text{ALLSYST}},$$

  where N_{chunk} is the number of tracers in the chunk considered.

- We then compute

$$w_{\rm comp}^{\rm PARTIAL} = w_{\rm FKP} \prod_{s \in \mathcal{S}'} w_s,$$

where $\mathcal{S}' \subseteq \mathcal{S}$ is the subset of systematic effects to be considered and $\mathcal{S} = \{\text{systot}, \ noz, \ cp\}$. In this case we compute the new effective number of tracers

$$n'_{eff} = \sum_{i=1}^{N_{chunk}} w_{{\rm comp},i}^{\rm PARTIAL}.$$

- Objects in the catalog with $w_{\rm comp}^{\rm PARTIAL} = 0$ or `veto` $= 0$ are removed. (ADD SECTION ON VETO MASKS?)
- We then normalize the completeness weights in each chunk by the corresponding n_{eff}/n'_{eff} to conserve the original effective number of tracers and avoid recomputing $n(z)$.

The study of systematic effects is relevant because it has been observed that voids are less sensitive to them (Kitaura et al., 2016; Liang et al., 2016), thus potentially helping in the improvement of constraints on the cosmological parameters currently determined from the matter tracer distribution.
Following the work in Zhao et al. (2016), the present work uses the DIVE code to generate void catalogs from a discrete set of matter tracers.

2.4 DIVE

The DIVE code is based on the Delaunay Triangulation (DT) algorithm (Delaunay, 1934), that divides the space in simplices and defines voids as the circumspheres within, which do not contain tracers (Zhao et al., 2016). The code returns a void catalog, composed of the comoving coordinates of the centers of the voids and the respective radii. Additionally, the efficiency allows for an easy scaling to a large number of galaxy catalogs, for instance, mock catalogs from simulations. This is useful for estimating the covariance matrices of clustering measurements. Unlike some of the methods briefly presented in the previous section, this approach does not depend on free parameters. This code is also convenient for the study of voids as tracers, since the output is a large catalog of void-centers that favors the statistical analysis of the population.

2.5 Types of voids

A study (Zhao et al., 2016) of the properties of DT voids, shows that the resulting catalog can be divided in two subsamples, according to the response of the number of voids in each category to the number of haloes. In particular, small spheres ($R < 8\,h^{-1}$Mpc) are correlated to the population of haloes, while big voids seem anticorrelated. The former are called *voids-in-clouds* due to their presence where matter density is higher, while on the other hand, big voids are called *voids-in-voids* since they are predominantly in empty regions of the cosmic web (Sheth et al., 2004).

Studies on the use of cosmic voids as tracers of under-densities for BAO peak detection (see Liang et al., 2016) have reached the conclusion that the *signal-to-noise ratio* (SNR) is maximized, in LRG (see section 2.6) voids, for a radius cut of $R \approx 16\,h^{-1}$Mpc.
Moreover, the number density of big voids has been shown to be independent on the galaxy density (Kitaura et al., 2016; Zhao et al., 2016), which has the most significant impact on the BAO measurements as shown by Ross et al. (2017). On the contrary, small voids, seem to provide redundant information on the galaxy distribution, given that they are mostly located in high matter density regions (Kitaura et al., 2016).

2.6 The eBOSS survey

The Extended Baryon Oscillation Spectroscopic Survey (eBOSS) started taking data in 2014, aiming towards a precise measurement of the BAO signal from various different matter tracers such as *Luminous Red Galaxies* (LRG), *Emission Line Galaxies* (ELG) and *Quasi-Stellar Objects* (QSO). These allow for the exploration of redshifts $z \in (0.6, 2.2)$ (Dawson et al., 2015).
The redshift coverage in the survey is divided as follows: LRG targets cover $z \in (0.6, 1)$, ELGs cover $z \in (0.6, 1.1)$ with 300 plates and QSO targets cover $z \in (0.8, 2.2)$. Observations are expected to take a similar time to complete as the BOSS, about 5400 hr (Dawson et al., 2015).
This work relies on the ELG part of the survey, whose redshift distribution is shown in figure AXAXZZX Notice that small voids are distributed around the peaks of the galaxy distribution, as would be expected since these are hidden within the cosmic clouds hence the name voids-in-clouds. On the contrary, the distribution of big voids has a valley around this maximum, this shows that this type of void is located in the emptier regions of the cosmic web. The shaded regions show the 1σ band provided by the 500 mock realizations used; which seem to be in good agreement with the observations.
As discussed in Raichoor et al. (2017), the target selection is dependent on some systematic effects such as stellar density, galactic extinction, or fiber collisions. Figure ASDASDS shows the geometry of the NGC zone of the survey.

3 Method

As mentioned before, this work uses ELG tracers: 87585 in the North Galactic Cap (NGC), and 109537 in the SGC. However, this dataset only accounts for a single realization of the Universe. It is then necessary to study a large number of mock datasets for each of these zones in order to estimate the covariance matrix. Ideally, the number of mocks should be significantly larger than the number of data points in the observed set, however, in this work we use 500 of these realizations. Each mock must share the properties of the observational data, such as geometry of the survey and galaxy density, as well as consistent clustering statistics.

3.1 Pipeline

For the observed dataset the pipeline is rather simple. The catalogs, given in sky coordinates (RA, DEC, z), are converted into comoving (X, Y, Z) ones. Then, DIVE is able to find the voids, resulting in a void catalog that contains the position (X, Y, Z) of the void center and its radius R. in order to compute the 2PCF, it is necessary to have a random catalog, though, for the case of voids this has to be created following the procedure described in Liang et al. (2016). On the other hand, for the mocks, the process is similar yet more time-consuming, given the large volume of data to process. In both cases, once DIVE is done generating the void catalogs, they should be converted to sky coordinates in order to apply the appropriate masks. To do this more efficiently, we tried to combine all catalogs into a single one, thus avoiding the repetitive and time-expensive reading of the masks for each mock. Once the voids inside the survey region were selected, we could generate the random void catalog in the following way, as sketched in Liang et al. (2016):

1. Combine 100 mock void catalogs for each zone.
2. Divide each file in z-bins with boundaries 0.6, 0.7, 0.8, 0.9, 1 , 1.1.
3. Divide each of the z-bins into R-bins with linearly spaced boundaries from 0 to 21 h^{-1}Mpc and bin size of 1. The last three bins are taken from 21 to 25, 25 to 30 and 30 to 50 h^{-1}Mpc.
4. Now, divide each of the resulting bins in two, one containing the RA, DEC and the other containing the z, R columns.
5. Shuffle in-place, the lines of one of the two halves.
6. Undo all the splitting, that is, combine the halves, then the R-bins and then the Z-bins.
7. Finally randomly choose some lines of the big random catalog left. In this case, We chose 2 700 000. When choosing lines we perform the radius cut, choosing objects with $R \in (R_c, 50\,h^{-1}\text{Mpc})$, with $R_c = 15.5\,h^{-1}$Mpc (see section 3.2).

Now, with the random catalog built, it is possible to compute the 2PCFs for voids. In order to do this, we use the Landy-Szalay estimator (Landy et al., 1993)

$$\xi = \frac{DD - 2DR + RR}{RR}. \tag{3}$$

When we consider the combined galaxy and void sample, this estimator conserves the form 3, however, each term has to be recomputed to account for both types of tracers as follows (Zhao et al., 2018)

$$DD = \frac{D_g D_g n_g^2 + 2D_g D_v n_g n_v w + D_v D_v n_v^2 w^2}{(n_g + n_v w)^2}, \tag{4}$$

$$DR = \frac{D_g R_g n_g^2 + D_v R_v n_v^2 w^2 + (D_g R_v + D_v R_g) n_g n_v w}{(n_g + n_v w)^2}, \tag{5}$$

$$RR = \frac{R_g R_g n_g^2 + 2R_g R_v n_g n_v w + R_v R_v n_v^2 w^2}{(n_g + n_v w)^2}. \tag{6}$$

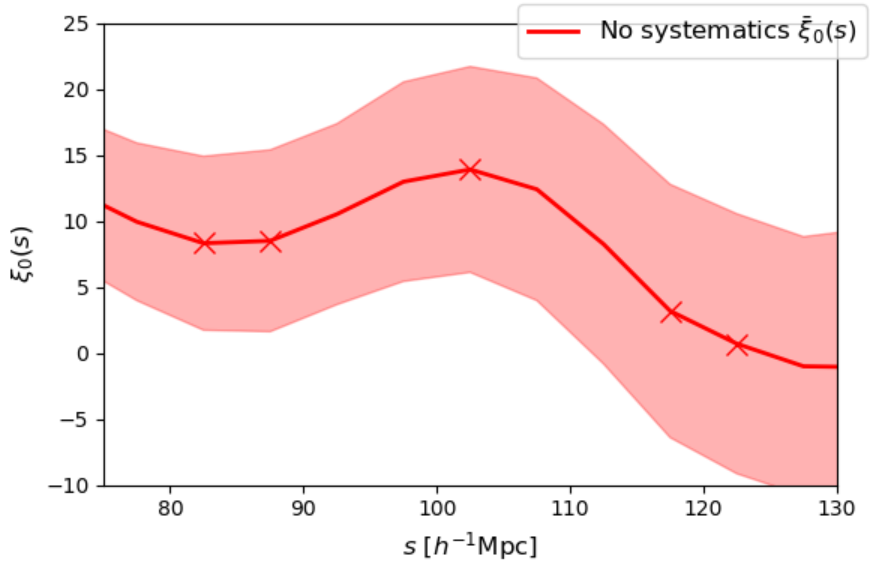

Figure 1: BAO feature on the mean of the 2PCF of mocks with no systematics along with the standard deviation (shaded region). Vertical lines show the values of $s_1^{\mathrm{dl}} = 82.5$, $s_2^{\mathrm{dl}} = 87.5$, $s_1^{\mathrm{BAO}} = 102.5$, $s_1^{\mathrm{dr}} = 117.5$ and $s_2^{\mathrm{dr}} = 122.5\,h^{-1}\mathrm{Mpc}$ respectively from left to right.

The new w parameter is introduced to prevent the negative BAO peak coming from the void-galaxy cross correlation 2PCF to weaken the galaxy BAO signal (Zhao et al., 2018). As described in Liang et al. (2016), Zhao et al. (2016) and Zhao et al. (2018) and mentioned earlier in this text, there are two types of DT voids, we will use $R_{big} > 16\,h^{-1}\mathrm{Mpc}$ and $R_{small} < 8\,h^{-1}\mathrm{Mpc}$. The latter are clearly voids in the geometrical sense, nonetheless, the local dark matter density contrast around them shows that these are actually rich in dark matter, while big voids are restricted to low local DM density contrast regions (see figure 9 in Zhao et al., 2016). These two cases should therefore be analyzed independently.

3.2 SNR analysis for BAO feature

In order to construct the void catalogs, we analyzed the Signal-to-noise ratio (SNR) of the BAO feature in the 2PCF. To do this, we followed the work done by Liang et al. (2016). To be precise, we generated 100 correlation functions for the catalogs with no systematics and computed the signal S defined as

$$S = \xi_0(s^{\mathrm{BAO}}) - \frac{\xi_0(s_1^{\mathrm{dl}}) + \xi_0(s_2^{\mathrm{dl}}) + \xi_0(s_1^{\mathrm{dr}}) + \xi_0(s_2^{\mathrm{dr}})}{4}, \tag{7}$$

where we have used $s_1^{\mathrm{BAO}} = 102.5$, $s_1^{\mathrm{dl}} = 82.5$, $s_2^{\mathrm{dl}} = 87.5$, $s_1^{\mathrm{dr}} = 117.5$ and $s_2^{\mathrm{dr}} = 122.5\,h^{-1}\mathrm{Mpc}$ as originally done by Liang et al. (2016). The location of these points can be seen in figure 1. The SNR is then

$$\mathrm{SNR}(R_c) = \frac{\langle S \rangle}{\sigma_S}, \tag{8}$$

with $\langle S \rangle$ the average signal over the 100 mocks used and σ_S the corresponding standard deviation. We did the test for different values of the low radius cut R_c. Figure 2 shows that the

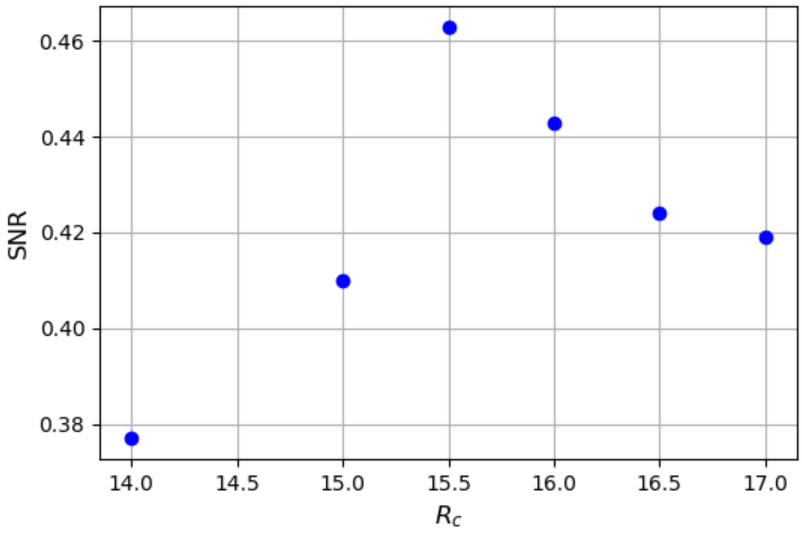

Figure 2: SNR vs low radius cut R_c. Upper cut is always set to $50\,h^{-1}$Mpc. Maximum SNR is obtained for $R_c = 15.5\,h^{-1}$Mpc.

SNR peaks at $R_c = 15.5\,h^{-1}$Mpc. Note that this is different from the optimal radius-cut given by the analysis by Liang et al. (2016). Their SNR was also much higher, with a maximum at SNR $\sim 10^1$.

3.3 Fitting procedure

3.3.1 The model

In section 3.1 we briefly outlined the necessary steps to generate the masked mock catalogs which include, for instance, coordinate conversions and computing distances. For these, a *fiducial cosmology* is necessary. The introduction of this cosmology implies that our measurements depend on it in such a way that we will actually look at how the BAO feature behaves in our data with respect to what is expected from the fiducial cosmology.
To fit the BAO feature we use the model proposed by Xu et al. (2012) to compute the 2PCF of the fiducial cosmology, ξ_t. This model relies on a generated template power spectrum, $P_t(k)$, which is then related to the model 2PCF via Fourier transform. As was done in Zhao et al. (2018), we include a Gaussian damping such that the model correlation function is

$$\xi_t(s) = \int \frac{k^2 \mathrm{d}k}{2\pi^2} \frac{\sin ks}{ks} P_t(k) \exp\left(-k^2 a^2\right), \tag{9}$$

where the parameter $a = 1\,h^{-1}$Mpc (Xu et al., 2012; Zhao et al., 2018). The function $P_t(k)$ is the template power spectrum. It is obtained via the relation

$$P_t(k) = [P_{\mathrm{lin}}(k) - P_{\mathrm{nw}}(k)] \exp\left(\frac{-\Sigma_{\mathrm{nl}}^2 k^2}{2}\right) + P_{\mathrm{nw}}(k). \tag{10}$$

The linear power spectrum $P_{\rm lin}$ is generated by CAMB software[1], while the *non-wiggle* power spectrum is computed from the baryonless transfer function as shown by Eisenstein et al. (1998). The first term in equation 10 describes the Gaussian dampening of the BAO feature (the *wiggles*) while the second term just reconstructs the power spectrum with the dampening taken into account.
Given that ξ_t describes the clustering of the fiducial cosmology, to perform our measurements we introduce the *model* 2PCF,

$$\xi_{\rm model}(s) \equiv B^2 \xi_t(\alpha s) + A(s), \tag{11}$$

which is the curve that should actually fit our data, given that it contains the parameters B and α along with the *nuisance parameters*, $a_i,\ i = 1, 2, 3$ contained in the polynomial

$$A(s) = \frac{a_1}{s^2} + \frac{a_2}{s} + a_3, \tag{12}$$

meant to fit the broadband spectrum of the data (Zhao et al., 2018). The other free parameters in the model are then B, for normalization, $\Sigma_{\rm nl}$ to account for the dampening of the BAO peak; and α, the dilation parameter. The latter contains the information on how the peak is shifted with respect to the fiducial cosmology used to build ξ_t.
Nonetheless, to fit voids it is necessary to modify this model. Zhao et al. (2018) found that the ratio between the tracer and linear non-wiggled power spectra showed a nontrivial behavior in the case of voids, while for galaxies it was almost flat. The non-linear behavior of such quantity is modeled by them as an extra quadratic term in k. The modified template spectrum is

$$P_t^v(k) = \left\{ [P_{\rm lin}(k) - P_{\rm nw}(k)] \exp\left(\frac{-\Sigma_{\rm nl}^2 k^2}{2} \right) + P_{\rm nw}(k) \right\} \{1 + ck^2\}, \tag{13}$$

where c is a seventh free parameter for the void fit.

3.3.2 Parameter inference

4 Results

4.1 ELG

5 Conclusion

[1] https://camb.info/

References

Delaunay, Boris (1934). "Sur la sphere vide". In: *Bulletin of the Academy of Sciences of the U. S. S. R. Classe des Sciences Mathematiques et Naturelles* 7, pp. 793–800.

Peebles, P. J. E. (Phillip James Edwin) (1980). *The large-scale structure of the universe*. Princeton University Press, p. 422. ISBN: 9780691082400.

Landy, Stephen D. and Alexander S. Szalay (July 1993). "Bias and variance of angular correlation functions". In: *The Astrophysical Journal* 412, p. 64. ISSN: 0004-637X. DOI: 10.1086/172900.

Eisenstein, Daniel and Wayne Hu (Sept. 1998). "Baryonic Features in the Matter Transfer Function". In: *The Astrophysical Journal* 496.2, pp. 605–614. ISSN: 0004-637X. DOI: 10.1086/305424.

Dodelson, Scott (2003). *Modern cosmology*. Academic Press. ISBN: 0122191412.

Sheth, Ravi K. and Rien van de Weygaert (May 2004). "A hierarchy of voids: much ado about nothing". In: *Monthly Notices of the Royal Astronomical Society* 350.2, pp. 517–538. ISSN: 00358711. DOI: 10.1111/j.1365-2966.2004.07661.x.

Colberg, Jörg M., Ravi K. Sheth, Antonaldo Diaferio, Liang Gao, and Naoki Yoshida (June 2005). "Voids in a ΛCDM universe". In: *Monthly Notices of the Royal Astronomical Society* 360.1, pp. 216–226. ISSN: 00358711. DOI: 10.1111/j.1365-2966.2005.09064.x.

Eisenstein, Daniel et al. (Nov. 2005). "Detection of the Baryon Acoustic Peak in the Large-Scale Correlation Function of SDSS Luminous Red Galaxies". In: *The Astrophysical Journal* 633.2, pp. 560–574. ISSN: 0004-637X. DOI: 10.1086/466512.

McDonald, Patrick and Daniel Eisenstein (July 2006). "Dark energy and curvature from a future baryonic acoustic oscillation survey using the Lyman-alpha forest". In: *Physical Review D* 76.6, p. 063009. ISSN: 1550-7998. DOI: 10.1103/PhysRevD.76.063009.

Eisenstein, Daniel, Hee-jong Seo, and Martin White (Aug. 2007). "On the Robustness of the Acoustic Scale in the Low-Redshift Clustering of Matter". In: *The Astrophysical Journal* 664.2, pp. 660–674. ISSN: 0004-637X. DOI: 10.1086/518755.

Hahn, Oliver, C. Marcella Carollo, Cristiano Porciani, and Avishai Dekel (Oct. 2007). "The evolution of dark matter halo properties in clusters, filaments, sheets and voids". In: *Monthly Notices of the Royal Astronomical Society* 381.1, pp. 41–51. ISSN: 0035-8711. DOI: 10.1111/j.1365-2966.2007.12249.x.

Forero-Romero, J. E., Y Hoffman, S. Gottlöber, A Klypin, and G Yepes (July 2009). "A dynamical classification of the cosmic web". In: *Monthly Notices of the Royal Astronomical Society* 396.3, pp. 1815–1824. ISSN: 00358711. DOI: 10.1111/j.1365-2966.2009.14885.x.

Komatsu, E et al. (Feb. 2009). "Five-year Wilkinson Microwave Anisotropy Probe observations: Cosmological interpretation". In: *Astrophysical Journal, Supplement Series* 180.2, pp. 330–376. ISSN: 00670049. DOI: 10.1088/0067-0049/180/2/330.

van de Weygaert, Rien and Willem Schaap (Aug. 2009). "The cosmic web: Geometric analysis". In: *Lecture Notes in Physics* 665.September, pp. 291–413. ISSN: 00758450. DOI: 10.1007/978-3-540-44767-2_11.

Bassett, Bruce A. and Renée Hlozek (2010). "Baryon Acoustic Oscillations". In: *Dark Energy: Observational and Theoretical Approaches*. Ed. by Pilar Ruiz-Lapuente. Cambridge University Press, pp. 246–276.

Abel, Tom, Oliver Hahn, and Ralf Kaehler (Nov. 2012). "Tracing the dark matter sheet in phase space". In: *Monthly Notices of the Royal Astronomical Society* 427.1, pp. 61–76. ISSN: 00358711. DOI: 10.1111/j.1365-2966.2012.21754.x.

Hong, T., J. L. Han, Z. L. Wen, L. Sun, and H. Zhan (Apr. 2012). "The correlation function of galaxy clusters and detection of baryon acoustic oscillations". In: *The Astrophysical Journal* 749.1, p. 81. ISSN: 0004-637X. DOI: 10.1088/0004-637X/749/1/81.

Xu, Xiaoying, Nikhil Padmanabhan, Daniel J. Eisenstein, Kushal T. Mehta, and Antonio J. Cuesta (2012). "A 2 per cent distance to z = 0.35 by reconstructing baryon acoustic oscillations - II. fitting techniques". In: *Monthly Notices of the Royal Astronomical Society* 427.3, pp. 2146–2167. ISSN: 00358711. DOI: 10.1111/j.1365-2966.2012.21573.x.

Weinberg, David H., Michael J. Mortonson, Daniel J. Eisenstein, Christopher Hirata, Adam G. Riess, and Eduardo Rozo (Sept. 2013). "Observational probes of cosmic acceleration". In: *Physics Reports* 530.2, pp. 87–255. ISSN: 03701573. DOI: 10.1016/j.physrep.2013.05.001.

Dawson, Kyle S et al. (Aug. 2015). "The SDSS-IV extended Baryon Oscillation Spectroscopic Survey: Overview and Early Data". In: *The Astronomical Journal* 151.2, p. 44. ISSN: 1538-3881. DOI: 10.3847/0004-6256/151/2/44.

Hong, Tao, J. L. Han, and Z. L. Wen (July 2016). "A detection of baryon acoustic oscillations from the distribution of galaxy clusters". In: *The Astrophysical Journal* 826.2, p. 154. ISSN: 1538-4357. DOI: 10.3847/0004-637X/826/2/154.

Kitaura, Francisco Shu et al. (2016). "Signatures of the Primordial Universe from Its Emptiness: Measurement of Baryon Acoustic Oscillations from Minima of the Density Field". In: *Physical Review Letters* 116.17. ISSN: 10797114. DOI: 10.1103/PhysRevLett.116.171301.

Liang, Yu, Cheng Zhao, Chia-Hsun Chuang, Francisco-Shu Kitaura, and Charling Tao (July 2016). "Measuring baryon acoustic oscillations from the clustering of voids". In: *Monthly Notices of the Royal Astronomical Society* 459.4, pp. 4020–4028. ISSN: 0035-8711. DOI: 10.1093/mnras/stw884.

Zhao, Cheng, Charling Tao, Yu Liang, Francisco-Shu Kitaura, and Chia-Hsun Chuang (July 2016). "DIVE in the cosmic web: voids with Delaunay triangulation from discrete matter tracer distributions". In: *Monthly Notices of the Royal Astronomical Society* 459.3, pp. 2670–2680. ISSN: 0035-8711. DOI: 10.1093/mnras/stw660.

Raichoor, A et al. (Nov. 2017). "The SDSS-IV extended Baryon Oscillation Spectroscopic Survey: final emission line galaxy target selection". In: *Monthly Notices of the Royal Astronomical Society* 471.4, pp. 3955–3973. ISSN: 0035-8711. DOI: 10.1093/mnras/stx1790.

Ross, Ashley J. et al. (2017). "The clustering of galaxies in the completed SDSS-III Baryon Oscillation Spectroscopic Survey: Observational systematics and baryon acoustic oscillations in the correlation function". In: *Monthly Notices of the Royal Astronomical Society* 464.1, pp. 1168–1191. ISSN: 13652966. DOI: 10.1093/mnras/stw2372.

Ata, Metin et al. (Feb. 2018). "The clustering of the SDSS-IV extended Baryon Oscillation Spectroscopic Survey DR14 quasar sample: first measurement of baryon acoustic oscillations between redshift 0.8 and 2.2". In: *Monthly Notices of the Royal Astronomical Society* 473.4, pp. 4773–4794. ISSN: 0035-8711. DOI: 10.1093/mnras/stx2630.

Zhao, Cheng, Chia-hsun Chuang, Francisco-shu Kitaura, Yu Liang, Marcos Pellejero-Ibanez, Charling Tao, Mariana Vargas-Magaña, Andrei Variu, and Gustavo Yepes (Feb. 2018). "Improving baryon acoustic oscillation measurement with the combination of cosmic voids and galaxies". In: 19.February, pp. 1–19.

Baumann, Daniel (n.d.). *Cosmology - Mathematical Tripos*.

Appendix

ELG tracer density distributions